Research article

Luca Moretti, Andrea Mazzanti, Arianna Rossetti, Andrea Schirato, Laura Polito, Fabio Pizzetti, Alessandro Sacchetti, Giulio Cerullo, Giuseppe Della Valle*, Filippo Rossi* and Margherita Maiuri*

Plasmonic control of drug release efficiency in agarose gel loaded with gold nanoparticle assemblies

Abstract: Plasmonic nanoparticles (NPs) are exploited to concentrate light, provide local heating and enhance drug release when coupled to smart polymers. However, the role of NP assembling in these processes is poorly investigated, although their superior performance as nanoheaters has been theoretically predicted since a decade. Here we report on a compound hydrogel (agarose and carbomer 974P) loaded with gold NPs of different configurations. We investigate the dynamics of light-heat conversion in these hybrid plasmonic nanomaterials via a combination of ultrafast pump-probe spectroscopy and hot-electrons dynamical modeling. The photothermal study ascertains the possibility to control the degree of assembling via surface functionalization of the NPs, thus enabling a tuning of the photothermal response of the plasmon-enhanced gel under continuous wave excitation. We exploit these assemblies to enhance photothermal release of drug mimetics with large steric hindrance loaded in the hydrogel. Using compounds with an effective hydrodynamic diameter bigger than the mesh size of the gel matrix, we find that the nanoheaters assemblies enable a two orders of magnitude faster cumulative drug release toward the surrounding environment compared to isolated NPs, under the same experimental conditions. Our results pave the way for a new paradigm of nanoplasmonic control over drug release.

Keywords: drug delivery; gold nanoparticles; hot electrons; nanoheaters; plasmonics; ultrafast spectroscopy.

*Corresponding authors: Giuseppe Della Valle, Dipartimento di Fisica, Politecnico di Milano, P.za Leonardo da Vinci 32, 20133, Milan, Italy; Istituto di Fotonica e Nanotecnologie, Consiglio Nazionale delle Ricerche, Piazza Leonardo da Vinci 32, 20133, Milan, Italy,
E-mail: giuseppe.dellavalle@polimi.it; Filippo Rossi, Dipartimento di Chimica, Materiali e Ingegneria Chimica "Giulio Natta", Politecnico di Milano, via Mancinelli 7, 20131 Milan, Italy,
E-mail: filippo.rossi@polimi.it; and Margherita Maiuri, Dipartimento di Fisica, Politecnico di Milano, P.za Leonardo da Vinci 32, 20133, Milan, Italy, E-mail: margherita.maiuri@polimi.it
Luca Moretti and Andrea Mazzanti, Dipartimento di Fisica, Politecnico di Milano, P.za Leonardo da Vinci 32, 20133, Milan, Italy
Arianna Rossetti, Fabio Pizzetti and Alessandro Sacchetti, Dipartimento di Chimica, Materiali e Ingegneria Chimica "Giulio Natta", Politecnico di Milano, via Mancinelli 7, 20131 Milan, Italy
Andrea Schirato, Dipartimento di Fisica, Politecnico di Milano, P.za Leonardo da Vinci 32, 20133, Milan, Italy; and Istituto Italiano di Tecnologia, via Morego 30, 16163, Genoa, Italy
Laura Polito, Consiglio Nazionale delle Ricerche, CNR-SCITEC, Via G. Fantoli 16/15, 20138, Milan, Italy
Giulio Cerullo, Dipartimento di Fisica, Politecnico di Milano, P.za Leonardo da Vinci 32, 20133, Milan, Italy; and Istituto di Fotonica e Nanotecnologie, Consiglio Nazionale delle Ricerche, Piazza Leonardo da Vinci 32, 20133, Milan, Italy. https://orcid.org/0000-0002-9534-2702

1 Introduction

The optical properties of metal nanoparticles (NPs), particularly their localized surface plasmon resonances (LSPRs), are well established [1–6]. It is now straightforward to design and fabricate high-quality metal NPs with tailored optical properties (such as optimized absorption, scattering coefficients and narrow LSPR bands) for multiple purposes, ranging from the detection of chemicals and biological molecules [7–11] to light-harvesting enhancement in solar cells [12–15] or applications in nanomedicine [16–19]. By dispersing the NPs in organic compounds (such as polymers) and creating a hybrid material, the robustness, responsiveness and flexibility of the system are enhanced, while preserving the intrinsic properties of the NPs [20]. Specifically, plasmonic nanostructures with high absorption cross sections are desirable for photothermal processes, such as cancer therapy [21] and drug and gene delivery [22].

The mechanism of heat release upon NP illumination is quite simple: the electromagnetic field of light excites the NPs LSPR (a collective motion of a large number of electrons) which rapidly decays nonradiatively into a distribution of hot electrons, which in turn thermalizes on the picosecond timescale with the phonons of the NP and converts the absorbed light into heat [4, 5]. Finally, heat is transferred from the NP to the environment through phonon-phonon interactions on a timescale of ~100 ps, increasing the temperature of the surrounding medium [7]. Heat generation by metal NPs under optical illumination has attracted much interest [23–34], and it has been demonstrated to enhance performances in the context of drug release [35]. In assemblies of NPs, collective effects can be used to strongly amplify the heating effect and to create local 'hot spots' featuring high temperature [36]. Although the superior performance of NPs assemblies (suprastructures) as nanoheaters has been theoretically predicted since a decade [36, 37], experimental studies of photothermal effects in such assemblies have so far been scarce [38].

The ability of gold (Au) NPs to be embedded in organic networks forming hybrids sensitive to light irradiation is well known in the literature [35, 39] and many research groups described the promising possibility of Au NPs loading within polymeric networks in order to improve cancer treatment [40], antimicrobial activity [41] or bone regeneration [42]; however, no similar studies employing NPs assemblies have been so far reported. Particularly promising biomaterial carriers are hydrogels, hydrophilic biocompatible three-dimensional networks, that found, among others applications in cartilage, central nervous system and bone repair strategies [43]. The hydrogels mild gelling condition and elastic properties allow their use as carriers for drugs and cells at the same time [43]. These features make these hydrogels good candidates for novel strategies in targeted/local delivery of specific drugs and biomolecules, to design advanced therapies for patients with severe or chronic diseases where the body's own response is not enough for the recovery of all functions [44]. By tuning the hydrogel swelling properties, degradation rate and cross-linking density, it is possible to smartly control cell fate and release rates. However, the extremely good results obtained as cell carriers [45] are not matched by similar results in drug delivery applications, both with hydrophobic and hydrophilic drugs [46].

In this paper we investigate photothermal effects in Au NPs assemblies loaded in a hydrogel compound and demonstrate that they enhance drug release performances. We test the photothermal properties of Au NPs assemblies incorporated in a hydrogel library already developed for cell-based therapies [47, 48] to ameliorate its drug delivery performance. In order to compare the drug release performances of isolated versus assembled Au NPs, in one case we decorate the NPs surface with polyethylene glycol (PEG) chains, commonly known as PEGylation, to guarantee that the Au NPs loaded in the gel remain isolated, in contrast with non-PEGylated Au NPs which tend to aggregate in suprastructures. First, we investigate the dynamics of light-heat conversion in these hybrid plasmonic nanomaterials via a combination of ultrafast pump-probe spectroscopy and hot-electrons dynamical modeling. The photothermal study ascertain the possibility to control the degree of assembling via PEGylation of the NPs, thus enabling a tuning of the photothermal response of the plasmon-enhanced gel under continuous wave excitation. Then, the obtained hybrid vehicle material is studied as drug delivery system with and without light irradiation, using a mimic for high steric hindrance therapeutic molecules.

Our results indicate that the presence or absence of PEGylation onto Au NPs can tune the final performance of the drug delivery devices. More specifically, we found that the nanoheaters assemblies enable two orders of magnitude increase of cumulative drug release of the hydrogel toward the surrounding environment compared to isolated NPs, under the same experimental conditions.

2 Materials and methods

2.1 Samples

The chosen hydrogel (HG) was obtained by synthesis from statistical block polycondensation between agarose and carbomer 974P (AC), together with cross-linkers [49]. In previous works, we observed that this HG can remain localized at the site of injection [48], showing high biocompatibility and good ability to provide viability of neural and mesenchymal stem cells together with pathology amelioration after spinal cord injury [50]. However, AC-based HGs are not light-responsive and so, after HG synthesis but before the sol/gel transition takes place, Au NPs were physically entrapped within the AC networks forming the organic-inorganic composite material. Au NPs synthetized with PEG capping (Au-PEG NPs) and in the absence of it were loaded in the HG. Then, the HG-NPs samples were loaded with two fluorescein-based compounds of different sizes, mimicking prototypical drugs: sodium fluorescein (SF) and fluorescein-dextran 70 kDa (DEX). The latter serves as a mimic for high steric hindrance therapeutic molecules like a wide class of proteins, such as anti-Cd11b antibodies, chondroitinase ABC and Anti-Nogo-A antibodies or erythropoietin [51]. We performed drug release experiments on SF-loaded and DEX-loaded HG-NPs in order to compare the efficiency in drug delivery applications of the hydrogels with Au NPs and Au-PEG NPs.

Details on NP synthesis procedures and gel characterization can be found in the Supplementary material.

2.2 Pump-probe measurements

Ultrafast pump-probe experiments were performed starting from a Ti:Sapphire chirped pulse amplified laser (Libra, Coherent), with 1 kHz repetition rate, central wavelength of 800 nm and pulse duration of ≈100 fs. The pump pulses at 400 nm were obtained by frequency doubling the laser output in a 1 mm β-barium borate crystal. Probe pulses in the visible spectral region (450–750 nm) were obtained by supercontinuum generation in a thin sapphire plate. The probe beam transmitted through the sample was detected by a high-speed spectrometer (Entwicklungsbuero EB Stresing). All samples were measured at room temperature in a 1-cm optical path plastic cuvette, filled with water and with the 2-mm-thin HG sample stuck on the cuvette inner wall. Measurements were processed with Matlab™ 2019a and Origin™ software.

2.3 Optical simulations

2.3.1 Steady-state quasi-static model:
The steady-state absorbance of the sample is calculated as $A = -\log_{10}(T)$, with $T = \exp(-\sigma_E N_p L)$ the transmission spectrum, retrieved from the extinction cross section σ_E of the considered nanostructures, their concentration, N_p (being 4×10^{11} and 5.6×10^{11} cm^{-3} for the isolated NPs, used to model the Au-PEG NPs, and for NP dimers, used to model the nanoassembled Au NPs samples, respectively), and the gel thickness $L = 2$ mm. The extinction cross section $\sigma_E = \sigma_A + \sigma_S$ is the sum of absorption cross section σ_A and scattering cross section σ_S, calculated under quasi-static approximation from the NP polarizability α. Further details on the model employed for the simulations and on the formulas used to calculate α, both in the case of Au-PEG NPs and non-PEGylated NPs, are reported in the Supplementary material Note 4.1.

2.3.2 The three-temperature model and photoinduced mechanical oscillations:
The transient optical model is based on the three-temperature (3TM) model [52, 53], describing the time evolution of the energetic internal degrees of freedom of plasmonic nanostructures upon ultrafast pulse illumination. The model solves for N, the excess energy stored in the nonthermal population of photoexcited electrons, Θ_e, the temperature of the thermalized hot electrons and Θ_l, the Au lattice temperature, and reads:

$$\frac{dN}{dt} = p_a(t) - aN - bN, \tag{1}$$

$$\gamma \Theta_e \frac{d\Theta_e}{dt} = aN - G(\Theta_e - \Theta_l), \tag{2}$$

$$C_l \frac{d\Theta_l}{dt} = bN + G(\Theta_e - \Theta_l) - G_a(\Theta_l - \Theta_m), \tag{3}$$

with Θ_m the surrounding environment (matrix) temperature. In the equations above, a and b are the high energy electron gas heating rate and the nonthermalized electrons-phonons scattering rate, respectively, G is the thermal electron-phonon coupling constant, and G_a a coupling coefficient (to be fitted on dynamical measurements) between Au phonons and the surrounding matrix phonons. Further details on these parameters can be found in the Supplementary material.

The 3TM has been then integrated with a mechanical oscillation model [54] for the expansion of the NP radius, here represented by parameter s, reading:

$$\frac{d^2s}{dt^2} + \frac{2}{\tau}\frac{ds}{dt} + \omega_0^2 s = \omega_0^2 \xi (\Theta_l - \Theta_0)R, \tag{4}$$

where $\xi = 1.5 \times 10^{-5}$ K^{-1} is the linear thermal expansion coefficient of gold [54], $\Theta_0 = 300$ K is the room temperature, ω_0 is the resonance frequency of the mechanical mode under consideration and τ is the oscillation damping time. The latter has been taken as a fitting parameter, whose value is set to $\tau = 16$ ps in order to correctly reproduce the damping of the mechanical oscillation observed in the non-PEGylated NPs sample. Regarding the resonance frequency, its expression has been adapted according to the investigated nanostructure, namely in the case of isolated NPs or NPs dimers modeling the assembled sample. Details on the two cases are provided in the Supplementary material.

2.3.3 Nonlinear optical model and transient extinction simulations:
We modeled the effect of the dynamical variables appearing in the 3TM on the ultrafast optical response following a segregated approach, reported by some of the authors of this work in the study by Zavelani-Rossi et al. [53], extensively validated and briefly outlined in the Supplementary material.

To model the transient optical response of the experimental samples, a further element affecting their transient permittivity, linked to the NPs thermal expansion and expressed in terms of the sphere stretching mode, needs to be accounted for. In this respect, the harmonic oscillator model outlined above [54] has been considered to act on the NP dimensions, changing the polarizability in a more direct way.

Thus, from the expression of the modified polarizability (refer to Supplementary material Note 4.3), in the quasi-static approximation, it is possible to define the extinction cross section as the sum of absorption and scattering cross section as follows:

$$\sigma_A(\lambda, t) = k \operatorname{Im}\{\alpha(\lambda, t)\}, \tag{5}$$

$$\sigma_S(\lambda, t) = \frac{k^4}{6\pi}|\alpha(\lambda, t)|^2, \tag{6}$$

$$\sigma_E(\lambda, t) = \sigma_A(\lambda, t) + \sigma_S(\lambda, t), \tag{7}$$

with k the probe wave-vector in the surrounding environment. Lastly, having defined the differential extinction cross section $\Delta\sigma_E(\lambda, t) = \sigma_E[\alpha(\lambda, t)] - \sigma_E[\alpha_0(\lambda)]$, where $\alpha_0(\lambda)$ is the unperturbed polarizability, the transient transmittance spectra are calculated as follows:

$$\frac{\Delta T}{T}(\lambda, t) = \exp[-\Delta\sigma_E(\lambda, t)N_P L] - 1. \tag{8}$$

2.4 Thermal simulations

To gain insight on the thermal behavior of the samples, a three-dimensional model has been built to solve the heat transfer problem and determine the temperature field (Θ) in the structure both in the time domain (for the pulsed optical excitation) and in the stationary regime (for CW illumination). The temperature Θ, solved for in the heat diffusion problem, is defined across the whole simulation domain. Therefore, $\Theta = \Theta_l$ within the Au NP, whereas $\Theta = \Theta_m$ in the surrounding environment (Θ_l and Θ_m having the same meaning as in Eqs. (1)–(3) above). The cases of a single isolated nanosphere and a $\mathcal{N} \times \mathcal{N}$ square array of sphere dimers have been investigated, with water as the surrounding environment in all simulations, its volume being varied so as to conserve the ratio of water and Au volumes. The general form of the heat transfer equation reads as follows:

$$\rho C_p \frac{\partial \Theta}{\partial t} - \kappa \nabla^2 \Theta = Q, \qquad (9)$$

where ρ, C_p and κ are the density, heat capacity and thermal conductivity of the considered material, respectively, and Q the heat source, which has been expressed according to the considered illumination conditions, being either in the pulsed (Q_p) or the CW (Q_c) regime. When solved in the steady state, the equations are formally analogous, with the temporal derivative vanishing. Supplementary material Note 4.4 provides details on the parameters used for the materials properties and thoroughly discusses case-by-case the expression used for the heat source in the four scenarios investigated, i.e., either pulsed or continuous illumination of either isolated or assembled NPs. The numerical analysis was performed using a commercial finite element method–based software (COMSOL Multiphysics 5.4).

2.5 Drug delivery experiment

The two compounds used for the drug delivery experiments (SF and DEX) were chosen mainly because of their steric hindrances, similar to many low steric hindrance drugs (SF) and high steric hindrance biomolecules (DEX), and because of their absorbance, that makes them easily detectable by UV spectroscopy. To perform the measurements, the compounds were mixed with HG-NPs gelling solution, above the sol/gel transition to allow good solute dispersion within the polymeric network. Gelation took place in steel cylinders (0.5 mL, $d = 1.1$ cm). Three samples for each condition (combination of compound and NPs) were put in excess of PBS and aliquots were collected at defined time points, while the sample volume was replaced by fresh PBS, in order to avoid mass-transfer equilibrium between the gel and the surrounding solution. The percentage of drug released was measured through UV spectroscopy [49]. In parallel, the same drug release studies were conducted on samples irradiated with a continuous wave UV laser diode centered at 375 nm (Omicron-Laserage Laserprodukte GmbH). The obtained release data were used to evaluate diffusion coefficients of the drug mimetic, following a previously described procedure [49] which models the delivery phenomenon with a Fickian behavior (further details are reported in the Supplementary material Note 2.4).

3 Results and discussions

3.1 Gold nanoparticles characterization

Figure 1A shows the schematic representation of the synthesis of Au NPs and PEGylated Au NPs (Au-PEG NPs). The procedure followed the Turkevich method, with the seeded-growth one-pot strategy (for a detailed description of the synthesis see Supplementary material) [55].

Figure 1B and C shows the measured absorption spectra of the two types of NPs. Au-PEG NPs (Figure 1B, continuous line) exhibit an absorption peak at 523 nm attributed to the typical LSPR of gold NPs of similar diameters ($\approx$20 nm) [1]. The absorption spectrum of the non-PEGylated NPs (Au NPs) (Figure 1C, continuous line) reveals a more complex
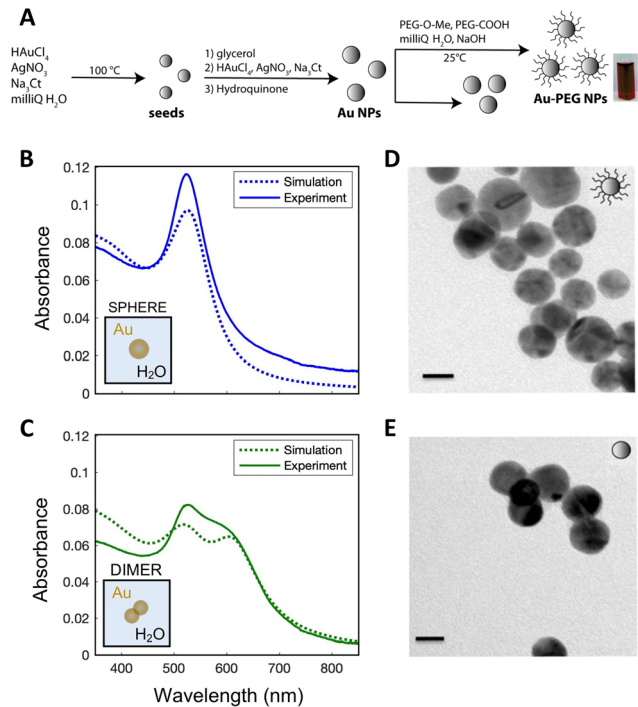

Figure 1: Schematic of the synthesis of gold nanoparticles (NPs) with and without polyethylene glycol (PEG) ligands (A). Absorption spectra of the gold NPs with (B) and without (C) PEG ligand, together with their respective simulated spectra (dashed lines). Corresponding transmission electron microscopy images of the two NPs (from a dried dispersion) with (D) and without (E) the ligand: the scale bar indicates a distance of 10 nm.

structure, with a main peak at 527 nm and a red-shifted broad shoulder. The presence of a second red-shifted band can be ascribed to a resonance caused by the aggregation of multiple NPs, forming NPs assemblies of larger dimensions whose interaction generates a collective plasmonic oscillation [2]. These assumptions are confirmed by the transmission electron microscopy (TEM) images (details in the Supplementary material) of the two samples of Au NPs (from dried dispersion): Figure 1D shows TEM image of the Au-PEG NPs where the NPs are well separated with an average diameter of 22 ± 2.8 nm, obtained from dynamic light scattering (DLS), while in Figure 1E the Au NPs (with an average diameter of 15 ± 1.6 nm, obtained from DLS) are in contact to each other, indicating a more pronounce tendency to assembling.

The absorption spectra were simulated by means of a quasi-static model [56], as detailed in the Materials and Methods section. The static absorption of Au-PEG NPs is correctly reproduced by a single gold sphere model (Figure 1B, dashed line) with 20 nm diameter free standing in water (the few nanometer thin PEG layer was disregarded because field penetration depth in the dielectric is

of the order of the optical wavelength). An increased Drude damping coefficient of $5\Gamma_0$ (Γ_0 being the Drude damping in bulk gold) was assumed in order to mimic the inhomogeneous broadening caused by size dispersion in the sample. The aggregated Au NPs were simulated by considering the simplest assembly configuration, a dimer of nanospheres with 15 nm diameter and a center-to-center distance of 11.7 nm (Figure 1C, dashed green line). Again, an increased Drude damping coefficient ($6.2\ \Gamma_0$) was assumed. The agreement with the experimental data is rather good, considering that a perfect match with the data should in fact include a distribution of different types of NPs assemblies (trimers or even bigger aggregates). Even though a precise determination of such distribution is beyond the scope of our study, the fact that the optical response is dominated by a dimeric contribution is a clear-cut indication of assembling in the non-PEGylated sample.

3.2 Tracking photothermal dynamics in plasmonic gels

We loaded the HG network with the two differently capped NPs (isolated and assembled NPs) and demonstrated that the NPs are trapped inside the organic matrix. This evidence was obtained by means of Fourier transform infrared and UV-Vis spectra of the loaded and nonloaded HGs (see Figure S2 of Supplementary material). The presence of Au NPs affects the swelling ratio and the mesh size of the HG depending on its temperature. However, the mechanical properties are preserved, remaining similar to the ones of its nonloaded counterpart (see Supplementary material Note 3 for further details). Then we performed ultrafast optical characterization of the two HG samples, with the aim of tracking the energy flow following photoexcitation and comparing their photothermal dynamics.

Figure 2 shows the 2D differential transmission ($\Delta T/T$) maps, as a function of probe wavelength and delay, acquired by exciting the NPs-HG samples with ≈0.17 mJ/cm² incident fluence at 400 nm pump wavelength. This wavelength, far from the plasmonic resonance of the samples, was selected in order to guarantee the same level of excitation (under the same pump fluence). Moreover, the two samples exhibit the same extinction coefficient at the chosen excitation wavelength, leading to a similar number of photogenerated excited carriers. This assumption is confirmed by the similar intensity of the $\Delta T/T$ peak signal (at 523 nm) at short time delays for the isolated NPs (Au-PEG NPs) and for the assembled ones (Au NPs), reported in Figure 2A and B, respectively. The $\Delta T/T$ signals up to 5 ps time delay for isolated NPs loaded in the HG
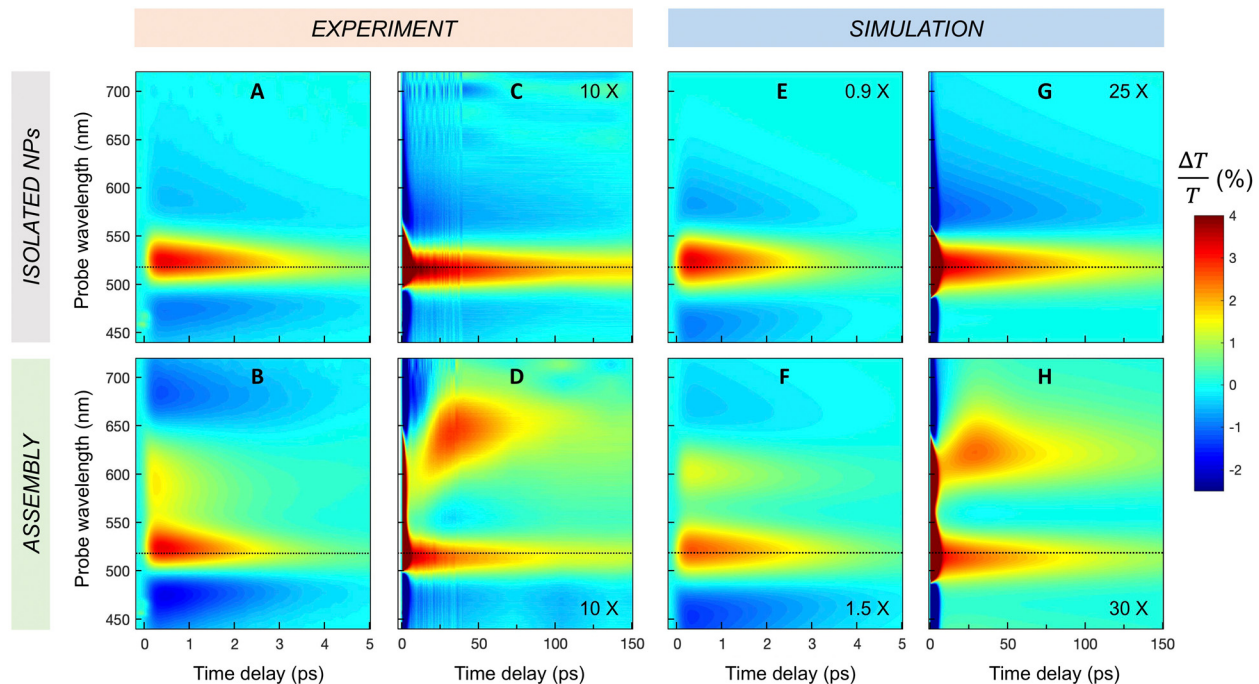

Figure 2: Experimental and simulated 2D $\Delta T/T$ maps of isolated and assembled nanostructures.
Experimental $\Delta T/T$ maps are obtained by pumping at 400 nm wavelength the HG containing Au-polyethylene glycol nanoparticles (PEG NPs) (A and C) and Au NPs (B and D). Panels E and G show simulated $\Delta T/T$ maps for isolated Au NPs, while panels F and H show simulated $\Delta T/T$ maps for a dimeric structure of Au NPs. Panels A, B, E and F show the 2D maps on the short time scale of the dynamics (up to 5 ps) with the same color scale. Panels C, D, G and H show the maps until 150 ps with a magnified $\Delta T/T$ scale in order to better distinguish the long time delay signals. Agreement between experimental and simulated data is remarkable both at short and long time delays.

(Figure 2A) is in perfect agreement with previous numerous works on the ultrafast transient response in similar plasmonic Au NPs [3–6]. The positive band peaked at 520 nm, and the two negative sidebands at longer and shorter wavelengths are due to the transient broadening of the quasi-static extinction peak of the nanosphere, caused by the pump-induced permittivity modulation that, in the considered range of wavelengths, is dominated by an increase of the imaginary part (see e.g., a study by Dal Conte et al. [57]). The $\Delta T/T$ map of the aggregated NPs (Figure 2B) still shows the strong band at 520 nm, with the same signal level, which is a confirmation of the hypothesis that the two samples have been loaded with approximately the same amount of plasmonic structures. However, in the HG with non-PEGylated NPs a second band, peaked at $\approx$590 nm, is clearly visible. This novel band is assigned to the fingerprint of the assembling, and in particular to the longitudinal plasmonic resonance of the NP dimer. To confirm this assignment, we also investigated the longer time scale of the dynamics. Figure 2C and D shows an expansion of the $\Delta T/T$ maps up to 150 ps (with a magnified signal scale). While Au-PEG NPs (Figure 2C) show a simple monotonic decay of the main plasmonic resonance, the non-PEGylated NPs (Figure 2D) show multiple spectral features. The signal of the longitudinal plasmonic resonance peaked at 590 nm shows a decay similar to the quasi-static resonance of the isolated nanosphere. However, a red-shifted positive band peaked at 647 nm appears at around 5 ps, reaching its maximum at ~30 ps time delay and then decaying over the 150 ps timescale, similarly to the plasmonic resonances.

Figure 2E–H shows the simulated $\Delta T/T$ maps for the two types of NPs, on the same timescales. Panels 2E and 2G show the simulated $\Delta T/T$ maps for an isolated gold nanosphere on a 5 and 150 ps time scale respectively: the agreement with Figure 2A and C (Au-PEG NPs) is remarkable. The simulated $\Delta T/T$ maps for the Au NPs sample (Figure 2F and H) were obtained by modeling the assembled NPs as a dimer composed of two gold nanospheres. At early times, the $\Delta T/T$ maps show two well distinct positive bands, related to transversal and longitudinal plasmonic resonances of the dimer, peaked at 521 and 598 nm, respectively (Figure 2F). At longer time delay (Figure 2H), the formation of a red-shifted band centered at 636 nm is clearly observable, with a maximum growth at around 35 ps. This behavior accurately reproduces the temporal and spectral evolution of the experimental signal detected at 647 nm. This band is related to the spectral response of the longitudinal resonance to the surrounding environment, which is modulated by the mechanical oscillation of the dimer on its stretching mode. This oscillation is coherently triggered in the ensemble of nanostructures by ultrafast heat transfer from the hot electrons to the gold

lattice via electron-phonon coupling, taking place on the few-ps time scale. Therefore, the temporal evolution of the signal at 647 nm is an indirect signature of the assembling configuration of the plasmonic structures, dominated by the dimer photothermal dynamics and subsequent modulation of the sample transmittance. The minor discrepancies in the spectral band position are justified by the approximation of the non-PEGylated Au NPs sample to an ensemble of dimers, which is likely not to account for the diverse combination of possible types of aggregates (with their own specific spectral and dynamical features) constituting in fact the experimental sample.

However, the dramatic contrast between the $\Delta T/T$ maps of PEGylated and non-PEGylated samples and the quantitative matching with numerical simulations demonstrate the suitability of ultrafast spectroscopy combined with nonlinear optical modeling for noninvasive analysis of the degree of assembling in plasmon loaded composite nanomaterials.

Interestingly, despite the different spectral features of the two samples in the $\Delta T/T$ maps, the relaxation dynamics both on the short timescale corresponding to electron-phonon coupling and on the longer time scale of phonon-phonon coupling (presiding over heat release to the water environment) looks rather similar. This is ascertained by direct comparison between the $\Delta T/T$ temporal traces at 520 nm wavelength, shown in Figure 3A–D. Experimental traces (black dotted curves) of panels A and C, recorded for the sample with PEGylated NPs, closely resemble the experimental traces of panels B and D, respectively, corresponding to the HG with non-PEGylated NPs. Moreover, the four measured traces are indeed in good agreement with simulations (red solid curves). Interestingly, the $\Delta T/T$ time traces on the few hundreds ps timescale precisely follow the dynamics of heat release to the water environment, retrieved by thermal simulations under the same pulsed regime of excitation, which is detailed by the red trace in Figure 3E and F for the isolated NPs and the NP assembly, respectively, (modeled as a 6×6 array of nanosphere dimers for simplicity). As a consequence, for ultrafast pulsed excitation, the temperature increase in the environment of the NPs is also the same in the two structures, and follows almost identical dynamics (blue and green traces in Figure 3E and F). Note that, even though our simple thermal model is not suitable for an accurate quantitative prediction of the temperature increase in our samples, the calculated temperature dynamics turned out to be very robust against variations of the internal arrangement of NPs within the assembly (see Figure S6 in the Supplementary material). However, as pointed out by Govorov et al. [36] in a seminal paper in 2006, plasmonic
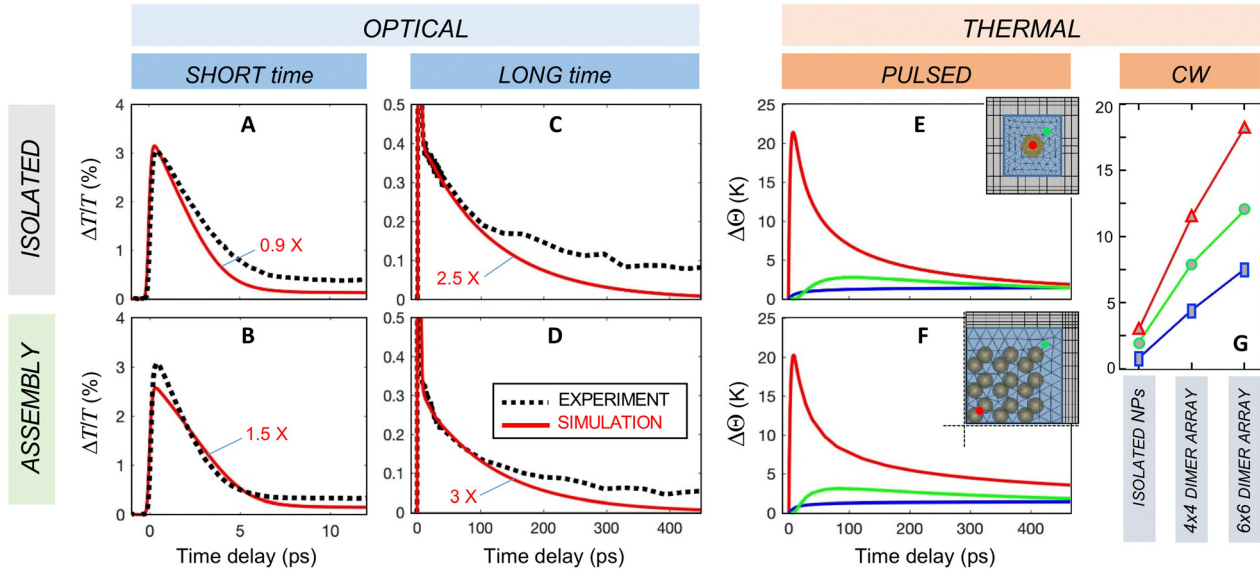
Figure 3: Experimental and simulated $\Delta T/T$ dynamics at 520 nm wavelength in HG samples containing Au-polyethylene glycol nanoparticles (PEG NPs) (A and C) and non-PEGylated Au NPs (B and D).
Panels A and B show the comparison till early times (12 ps) while panels C and D show the dynamics till 450 ps. Panels E, F and G report the results of thermal simulations. Panel E and F show the evolution of the temperatures due to impulsive excitation (as in ultrafast pump-probe experiments) in isolated Au NPs and in a 6×6 array of Au NP dimers. Red and green traces are the temperature increase in two selected points of the domain, highlighted with the same color coding in the insets (showing the geometry and mesh used in the simulations, with the first quadrant only, in panel F, for better reading), while blue trace is the average temperature increase of the water domain (10 times magnified for better reading). Panel G shows the temperature increase in the same spots but under continuous wave excitation corresponding to an input laser intensity $I_0 = 10^5$ W/cm², which is a typical excitation level assumed when modeling plasmonic nanoheaters in an open domain of water environment [36].

assemblies can behave as very efficient nanoheaters, out-performing isolated nanostructures under illumination with longer pulses. More precisely, one needs a pulse duration τ exceeding the heat diffusion time T across the whole size of the assembly. According to a study by Govorov et al. [36], for an assembly of size l, the heat diffusion time can be estimated as $T = l^2/K_m$, with $K_m = \kappa/(\rho C_p)$ the thermal diffusivity of the matrix embedding the NPs of the assembly. In our case of a water matrix, we obtain $K_m = 1.43 \times 10^{-7}$ m²/s, and thus $T \simeq 0.3$ μs, for a nano-assembly with $l \simeq 200$ nm. This increased efficiency is mostly related to the cumulative effect deriving from the addition of more heat fluxes with the increasing number of NPs (plus, possibly, the Coulomb interaction between the NPs which is driven by plasmon-enhanced electric fields and depends on NPs distances and arrangements [37]). To ascertain this point, we performed thermal simulations under continuous wave excitation. The results are reported in Figure 3G for three different configurations of NPs: iso-lated nanospheres, a 4×4 and a 6×6 array of nanosphere dimers. Our simulations confirm the dramatic improve-ment of local heating performances for the assembly if compared to isolated structures, in agreement with the

scaling law for peak temperature increase reported in a study by Govorov et al. [36]. For a further validation of this picture, we also performed thermal simulations for two systems having exactly the same number of NPs (25 dimers) distributed in the same volume of water, but with two very different degrees of assembling. We found that, even though the average temperature in the water volume is basically the same (because of the same thermal loading of the individual NPs), the temperature in the center of the metallic dimer and close to the edge of the assembly dramatically increases with the degree of assembling (see Figure S7 in the Supplementary material).

3.3 Photothermal drug release study

The outcomes of the optical and photothermal studies detailed above indicate that the degree of plasmonic assembling in the two HGs loaded with PEG or non-PEG NPs is substantially different, and that the non-PEGylated sample is expected to be much more efficient in generating a photothermal effect under CW illumination, compared to the PEGylated one. Since this HG has been demonstrated to

behave as an efficient vector for stem cells [48], it is of great interest to test it together with the two classes of NPs as a drug photothermal vector, and to compare the different drug release efficiencies as a function of the degree of plasmonic assembling.

To test the efficacy of the NPs-HG as vehicle for drug delivery, we chose two different types of compounds to be released: (i) SF, (hydrodynamic diameter = 0.07 nm), a small steric hindrance drug mimetic with an effective diameter which is smaller than the HG mesh size, and (ii) DEX (hydrodynamic diameter = 8 nm), a big steric hindrance drug mimetic, which is instead of comparable size to the HG mean mesh size. To perform drug release experiments under photothermal excitation, we used a CW UV diode laser source (375 nm emission wavelength) and we measured the percentage of drug release after fixed temporal intervals under illumination with 10 W/cm^2 intensity. Figure 4A and B schematize the results of our experiments. Under illumination, NPs absorb light and release heat to the surrounding HG matrix, producing an expansion in the mesh size and thus creating more space for the drug to freely move and to be released outside the HG. Generally, for drugs with a size smaller than the HG mesh size, we expect no difference in the release performances between irradiated and non-irradiated samples, since the drug can always escape the HG matrix

(Figure 4A). On the other hand, bulky drugs should be stuck between the HG meshes and therefore be released only under illumination conditions (Figure 4B). Similar results to those obtained without irradiation (red symbols in Figure 4C and E) were also observed by irradiating the HG network without Au NPs and not reported in the same Figure for clarity reason (trends in Supplementary material Figure S5), confirming the key role of the Au NPs in the HG network for photothermal drug release.

Figure 4C shows the results of the cumulative release experiments for SF in three conditions: (i) no illumination (red squares); (ii) illumination of the Au-PEG NPs HG (empty squares); (iii) illumination of the non-PEGylated NPs HG (black squares). It is clear that the release of the SF is independent of both the irradiation and the type of NPs used, since data are showing very similar trends. Due to its small size, the release is always allowed, since the drug is not retained by the meshes of the HG even in the non-irradiated (cold and tight) condition. The situation drastically changes if we analyze the cumulative release experiments of the DEX case under the same conditions (Figure 4E). The release of DEX is mostly not allowed in absence of irradiation, keeping a value below 5% all the time. This result is due to the trapping of the large drug in the meshes of the gel. On the other hand, when the NPs-HG is illuminated, a striking distinction between the two types
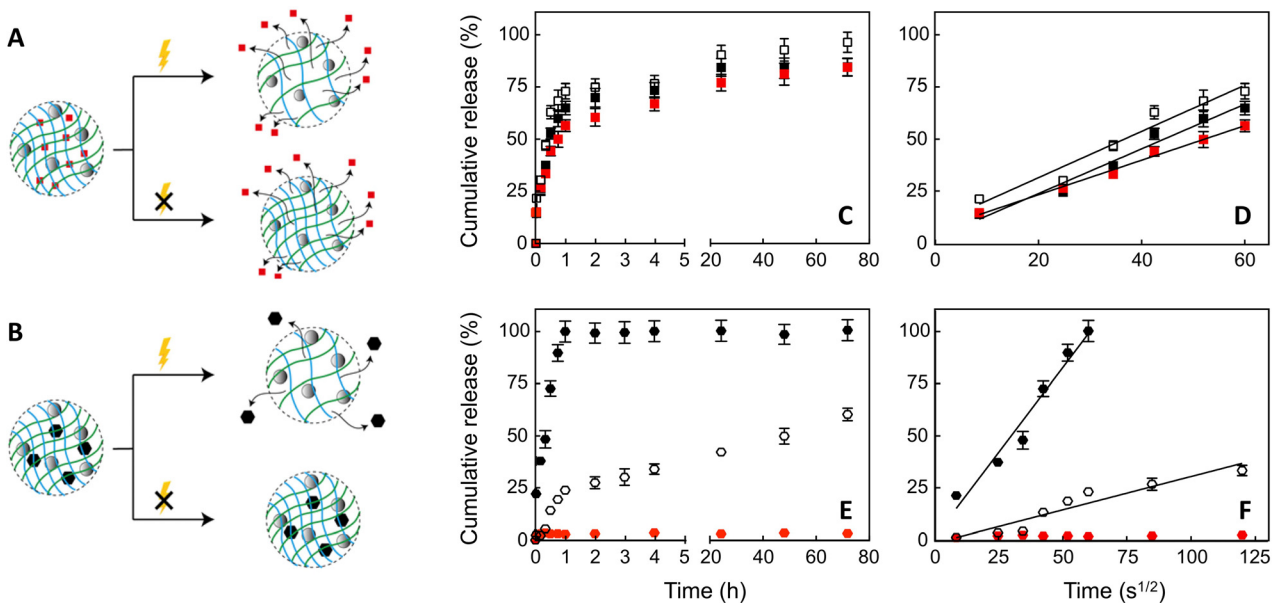

Figure 4: Comparison of NPs-HG with insertion of sodium fluorescein (SF) (A) and fluorescein-dextran 70 kDa (DEX) (B), with and without heating by a continuous UV laser.
Cumulative release of the drug in three different conditions: no irradiation of the pristine HG (red symbols), irradiation of the HG with Au-polyethylene glycol nanoparticles (PEG NPs) (empty symbols), irradiation of the HG with non-PEGylated NPs (black symbols). The cumulative release is shown as function of continuous illumination temporal interval (hours) for SF (C) and DEX (E). Panels (D) and (F) show the corresponding magnified short time interval in square root of seconds in order to extrapolate the diffusion coefficient [49].

of NPs used is observed. The release is clearly present in both cases, in agreement with a mesh size modification due to a local temperature increase (data not shown); however the amount of compound released and the release rate are quite different. In Au-PEG NPs HG, the release reaches 25% within 1 h of illumination and then slowly grows in the whole investigated time range without reaching 100% (Figure 4E, empty hexagons). For the Au NPs HG, the release reaches ~100% value in the first hour of illumination (Figure 4E, black hexagons), after which it saturates. These results confirm the enhancement in nanoheating for plasmonic NP assemblies: aggregated Au NPs contribute to a faster heating of the HG matrix by controlling the drug release in terms of speed and amount. To better investigate and understand the influence of illumination, we plotted the percentage of release against the square root of time (see Figure 4D and F), where a linear relationship is indicative of Fickian diffusion. Figure 4D shows that Fickian diffusion for SF release lasts for about 1 h and then reaches a plateau. The initial burst release is around 20% and almost no differences are visible between the three cases. Diffusion coefficients were calculated using a Fick-based model with cylindrical geometry already validated in literature [58] (details in Supplementary material) and their values are around 1.5×10^{-8} m^2/s, for both neat HG and Au NPs loaded ones. Considering DEX release (Figure 4F), three different cases in terms of Fickian diffusion duration are observed: no Fickian diffusion for neat HG, 1 h for Au NPs (corresponding to a timescale of 60 s$^{1/2}$ in the figure) and about 4 h for Au-PEG NPs (corresponding to 120 s$^{1/2}$). Also burst release presents differences: around 18% for Au NPs and almost negligible for Au-PEG NPs. In accordance, the calculated diffusion coefficients are 2.5×10^{-8} m^2/s for Au NPs and 1.7×10^{-10} m^2/s for Au-PEG NPs.

This set of experiments confirms that the presence of Au NPs influences the release of compounds with effective hydrodynamic diameters bigger than the mesh size of the host matrix. Moreover, we found that the aggregated Au NPs show a much more efficient heat release towards the surrounding environment.

4 Conclusion

In this study, we have investigated the properties of gold NPs, incorporated in a hydrogel matrix, as photothermal agents promoting light-assisted release of drugs with size bigger than the hydrogel mesh size. We have compared NPs capped with PEG chains to uncapped NPs. We have found that PEGylation prevents aggregation of the NPs, which thus behave as isolated nanostructures, while the absence of surface functionalization leads to their aggregation, forming suprastructures which, to a first approximation, can be described as assemblies of dimers. Ultrafast transient absorption spectroscopy, in combination with simulations of the transient optical response, was used to compare isolated and aggregated nanostructures. Experiments, in excellent agreement with the simulations, revealed significant differences between PEGylated and uncapped NPs, allowing to retrieve the characteristic spectral signatures of dimerization. The difference between capped and uncapped NPs was confirmed in photothermal drug release studies, in which the hydrogel, loaded with the NPs as well as with a molecule (fluorescein-dextran 70 kDa) mimicking drugs with big steric hindrance, was subjected to continuous wave UV illumination. A dramatic difference was observed between the photothermal performance of the aggregated and the isolated NPs, with a measured two order of magnitude higher diffusion coefficient for the former with respect to the latter.

Taken together, these results confirm the theoretical prediction that NP assemblies act as efficient nanoheaters, greatly increasing the efficiency of the photothermal effect with respect to isolated NPs because of the cumulative effect of heat fluxes. This is particularly effective in hydrogels loaded with plasmonic nanoassemblies because the breaking of the polymeric network of the gel is mostly sensitive to thermal spots driven at higher temperatures, rather than to a more uniform but moderate heating of the whole matrix, achievable with isolated NPs. The importance of these results is twofold. On the one hand, they open up a new paradigm for nanoplasmonic control over drug release, where the aggregation of the nanostructures can be used as additional degree of freedom to control the efficiency of the process. On the other hand, since the specific agarose-carbomer hydrogel used in these studies has proven to be an effective vector for stem cells, it will be interesting in the future to investigate its performance as a photothermal drug vector.

References

[1] P. K. Jain, K. S. Lee, I. H. El-Sayed, and M. A. El-Sayed, "Calculated absorption and scattering properties of gold nanoparticles of different size, shape, and composition: applications in biological imaging and biomedicine," *J. Phys. Chem. B*, vol. 110, pp. 7238–7248, 2006.

[2] S. K. Ghosh and T. Pal, "Interparticle coupling effect on the surface plasmon resonance of gold nanoparticles: from theory to applications," *Chem. Rev.*, vol. 107, pp. 4797–4862, 2007.

[3] J. H. Hodak, A. Henglein, and G. V. Hartland, "Size dependent properties of Au particles: coherent excitation and dephasing of acoustic vibrational modes," *J. Chem. Phys.*, vol. 111, pp. 8613–8621, 1999.

[4] O. L. Muskens, N. Del Fatti, and F. Vallée, "Femtosecond response of a single metal nanoparticle," *Nano Lett.*, vol. 6, pp. 552–556, 2006.

[5] T. S. Ahmadi, S. L. Logunov, and M. A. El-Sayed, "Picosecond dynamics of colloidal gold nanoparticles," *J. Phys. Chem.*, vol. 100, pp. 8053–8056, 1996.

[6] G. V. Hartland, "Coherent excitation of vibrational modes in metallic nanoparticles," *Annu. Rev. Phys. Chem.*, vol. 57, pp. 403–430, 2006.

[7] P. K. Jain, X. Huang, I. H. El-Sayed, and M. A. El-Sayed, "Noble metals on the nanoscale: optical and photothermal properties and some applications in imaging, sensing, biology, and medicine," *Acc. Chem. Res.*, vol. 41, pp. 1578–1586, 2008.

[8] H. Jans and Q. Huo, "Gold nanoparticle-enabled biological and chemical detection and analysis," *Chem. Soc. Rev.*, vol. 41, pp. 2849–2866, 2012.

[9] P. Da, W. Li, X. Lin, Y. Wang, J. Tang, and G. Zheng, "Surface plasmon resonance enhanced real-time photoelectrochemical protein sensing by gold nanoparticle-decorated TiO$_2$ nanowires," *Anal. Chem.*, vol. 86, pp. 6633–6639, 2014.

[10] C. Wang, and C. Yu, "Detection of chemical pollutants in water using gold nanoparticles as sensors: a review," *Rev. Anal. Chem.*, vol. 32, pp. 1–14, 2013.

[11] I. Ament, J. Prasad, A. Henkel, S. Schmachtel, and C. Sönnichsen, "Single unlabeled protein detection on individual plasmonic nanoparticles," *Nano Lett.*, vol. 12, pp. 1092–1095, 2012.

[12] S. Carretero-Palacios, A. Jiménez-Solano, and H. Míguez, "Plasmonic nanoparticles as light-harvesting enhancers in perovskite solar cells: a user's guide," *ACS Energy Lett.*, vol. 1, pp. 323–331, 2016.

[13] S. Muduli, O. Game, V. Dhas, et al., "TiO2–Au plasmonic nanocomposite for enhanced dye-sensitized solar cell (DSSC) performance," *Sol. Energy*, vol. 86, pp. 1428–1434, 2012.

[14] X. Dang, J. Qi, M. T. Klug, et al., "Tunable localized surface plasmon-enabled broadband light-harvesting enhancement for high-efficiency panchromatic dye-sensitized solar cells," *Nano Lett.*, vol. 13, pp. 637–642, 2013.

[15] S. Chang, Q. Li, X. Xiao, K. Y. Wong, and T. Chen, "Enhancement of low energy sunlight harvesting in dye-sensitized solar cells using plasmonic gold nanorods," *Energy Environ. Sci.*, vol. 5, p. 9444, 2012.

[16] I. Willner, "Stimuli-controlled hydrogels and their applications," *Acc. Chem. Res.*, vol. 50, pp. 657–658, 2017.

[17] M. Wei, Y. Gao, X. Li, and M. J. Serpe, "Stimuli-responsive polymers and their applications," *Polym. Chem.*, vol. 8, pp. 127–143, 2017.

[18] D. A. Urban, L. Rodriguez-Lorenzo, S. Balog, C. Kinnear, B. Rothen-Rutishauser, and A. Petri-Fink, "Plasmonic nanoparticles and their characterization in physiological fluids," *Colloids Surf. B Biointerfaces*, vol. 137, pp. 39–49, 2016.

[19] V. Hirsch, C. Kinnear, M. Moniatte, B. Rothen-Rutishauser, M. J. D. Clift, and A. Fink, "Surface charge of polymer coated SPIONs influences the serum protein adsorption, colloidal stability and subsequent cell interaction in vitro," *Nanoscale*, vol. 5, p. 3723, 2013.

[20] I. Pastoriza-Santos, C. Kinnear, J. Pérez-Juste, P. Mulvaney, and L. M. Liz-Marzán, "Plasmonic polymer nanocomposites," *Nat. Rev. Mater.*, vol. 3, pp. 375–391, 2018.

[21] N. S. Abadeer, and C. J. Murphy, "Recent progress in cancer thermal therapy using gold nanoparticles," *J. Phys. Chem. C*, vol. 120, pp. 4691–4716, 2016.

[22] Y. Wang and D. S. Kohane, "External triggering and triggered targeting strategies for drug delivery," *Nat. Rev. Mater.*, vol. 2, p. 17020, 2017.

[23] H. H. Richardson, Z. N. Hickman, A. O. Govorov, A. C. Thomas, W. Zhang, and M. E. Kordesch, "Thermooptical properties of gold nanoparticles embedded in ice: characterization of heat generation and melting," *Nano Lett.*, vol. 6, pp. 783–788, 2006.

[24] T. Teranishi, S. Hasegawa, T. Shimizu, and M. Miyake, "Heat-induced size evolution of gold nanoparticles in the solid state," *Adv. Mater.*, vol. 13, pp. 1699–1701, 2001.

[25] D. Pissuwan, S. M. Valenzuela, and M. B. Cortie, "Therapeutic possibilities of plasmonically heated gold nanoparticles," *Trends Biotechnol.*, vol. 24, pp. 62–67, 2006.

[26] K. Akamatsu and S. Deki, "TEM investigation and electron diffraction study on dispersion of gold nanoparticles into a nylon 11 thin film during heat treatment," *J. Colloid Interface Sci.*, vol. 214, pp. 353–361, 1999.

[27] K. Akamatsu and S. Deki, "Dispersion of gold nanoparticles into a nylon 11 thin film during heat treatment: in situ optical transmission study," *J. Mater. Chem.*, vol. 8, pp. 637–640, 1998.

[28] T. Shimizu, T. Teranishi, S. Hasegawa, and M. Miyake, "Size evolution of alkanethiol-protected gold nanoparticles by heat treatment in the solid state," *J. Phys. Chem. B*, vol. 107, pp. 2719–2724, 2003.

[29] B. El Roustom, G. Fóti, and C. Comninellis, "Preparation of gold nanoparticles by heat treatment of sputter deposited gold on boron-doped diamond film electrode," *Electrochem. Commun.*, vol. 7, pp. 398–405, 2005.

[30] C. Y. Tsai, H. T. Chien, P. P. Ding, B. Chan, T. Y. Luh, and P. H. Chen, "Effect of structural character of gold nanoparticles in nanofluid on heat pipe thermal performance," *Mater. Lett.*, vol. 58, pp. 1461–1465, 2004.

[31] X. Sun, X. Jiang, S. Dong, and E. Wang, "One-step synthesis and size control of dendrimer-protected gold nanoparticles: a heat-treatment-based strategy," *Macromol. Rapid Commun.*, vol. 24, pp. 1024–1028, 2003.

[32] A. Plech, V. Kotaidis, S. Grésillon, C. Dahmen, and G. von Plessen, "Laser-induced heating and melting of gold nanoparticles studied by time-resolved x-ray scattering," *Phys. Rev. B*, vol. 70, p. 195423, 2004.

[33] M. Hu, X. Wang, G. V. Hartland, V. Salgueiriño-Maceira, and L. M. Liz-Marzán, "Heat dissipation in gold–silica core-shell nanoparticles," *Chem. Phys. Lett.*, vol. 372, pp. 767–772, 2003.

[34] M. M. Maye, W. Zheng, F. L. Leibowitz, N. K. Ly, and C-J. Zhong, "Heating-induced evolution of thiolate-encapsulated gold nanoparticles: a strategy for size and shape manipulations," *Langmuir*, vol. 16, pp. 490–497, 2000.

[35] A. J. Gormley, N. Larson, S. Sadekar, R. Robinson, A. Ray, and H. Ghandehari, "Guided delivery of polymer therapeutics using plasmonic photothermal therapy," *Nano Today*, vol. 7, pp. 158–167, 2012.

[36] A. Mazzanti, Z. Yang, M. G. Silva, et al., "Light–heat conversion dynamics in highly diversified water-dispersed hydrophobic nanocrystal assemblies," *Proc. Natl. Acad. Sci. U. S. A.*, vol. 116, pp. 8161–8166, 2019.

[37] E. R. Ruskowitz and C. A. DeForest, "Photoresponsive biomaterials for targeted drug delivery and 4D cell culture," *Nat. Rev. Mater.*, vol. 3, p. 17087, 2018.

[38] S.-W. Lv, Y. Liu, M. Xie, et al., "Near-infrared light-responsive hydrogel for specific recognition and photothermal site-release of circulating tumor cells," *ACS Nano*, vol. 10, pp. 6201–6210, 2016.

[39] S. C. T. Moorcroft, L. Roach, D. G. Jayne, Z. Y. Ong, and S. D. Evans, "Nanoparticle-loaded hydrogel for the light-activated release and photothermal enhancement of antimicrobial peptides," *ACS Appl. Mater. Interfaces*, vol. 12, pp. 24544–24554, 2020.

[40] D. N. Heo, W.-K. Ko, M. S. Bae, et al., "Enhanced bone regeneration with a gold nanoparticle–hydrogel complex," *J. Mater. Chem. B*, vol. 2, pp. 1584–1593, 2014.

[41] X. Fu, L. Hosta-Rigau, R. Chandrawati, and J. Cui, "Multi-stimuli-responsive polymer particles, films, and hydrogels for drug delivery," *Inside Chem.*, vol. 4, pp. 2084–2107, 2018.

[42] B. V. Slaughter, S. S. Khurshid, O. Z. Fisher, A. Khademhosseini, and N. A. Peppas, "Hydrogels in regenerative medicine," *Adv. Mater.*, vol. 21, pp. 3307–3329, 2009.

[43] P. M. Kharkar, K. L. Kiick, and A. M. Kloxin, "Designing degradable hydrogels for orthogonal control of cell microenvironments," *Chem. Soc. Rev.*, vol. 42, pp. 7335–7372, 2013.

[44] E. Mauri, F. Rossi, and A. Sacchetti, "Tunable drug delivery using chemoselective functionalization of hydrogels," *Mater. Sci. Eng. C*, vol. 61, pp. 851–857, 2016.

[45] I. Caron, F. Rossi, S. Papa, et al., "A new three dimensional biomimetic hydrogel to deliver factors secreted by human mesenchymal stem cells in spinal cord injury," *Biomaterials*, vol. 75, pp. 135–147, 2016.

[46] G. Perale, F. Rossi, M. Santoro, et al., "Multiple drug delivery hydrogel system for spinal cord injury repair strategies," *J. Contr. Release*, vol. 159, pp. 271–280, 2012.

[47] M. Santoro, P. Marchetti, F. Rossi, et al., "Smart approach to evaluate drug diffusivity in injectable Agar–Carbomer hydrogels for drug delivery," *J. Phys. Chem. B*, vol. 115, pp. 2503–2510, 2011.

[48] S. Papa, I. Vismara, A. Mariani, et al., "Mesenchymal stem cells encapsulated into biomimetic hydrogel scaffold gradually release CCL2 chemokine in situ preserving cytoarchitecture and promoting functional recovery in spinal cord injury," *J. Contr. Release*, vol. 278, pp. 49–56, 2018.

[49] B. K. Kwon, E. B. Okon, W. Plunet, et al., "A systematic review of directly applied biologic therapies for acute spinal cord injury," *J. Neurotrauma*, vol. 28, pp. 1589–1610, 2011.

[50] C.-K. Sun, F. Vallée, L. H. Acioli, E. P. Ippen, and J. G. Fujimoto, "Femtosecond-tunable measurement of electron thermalization in gold," *Phys. Rev. B*, vol. 50, pp. 15337–15348, 1994.

[51] M. Zavelani-Rossi, D. Polli, S. Kochtcheev, et al., "Transient optical response of a single gold nanoantenna: the role of plasmon detuning," *ACS Photonics*, vol. 2, pp. 521–529, 2015.

[52] G. V. Hartland, "Optical studies of dynamics in noble metal nanostructures," *Chem. Rev.*, vol. 111, pp. 3858–3887, 2011.

[53] A. Silvestri, V. Zambelli, A. M. Ferretti, D. Salerno, G. Bellani, and L. Polito, "Design of functionalized gold nanoparticle probes for computed tomography imaging," *Contrast Media Mol. Imaging*, vol. 11, pp. 405–414, 2016.

[54] S. A. Maier, *Plasmonics: Fundamentals and Applications*, New York, Springer Science, 2007.

[55] S. Dal Conte, M. Conforti, D. Petti, et al., "Disentangling electrons and lattice nonlinear optical response in metal-dielectric Bragg filters," *Phys. Rev. B*, vol. 89, p. 125122, 2014.

[56] F. Rossi, R. Ferrari, S. Papa, et al., "Tunable hydrogel—nanoparticles release system for sustained combination therapies in the spinal cord," *Colloids Surf. B Biointerfaces*, vol. 108, pp. 169–177, 2013.